

Nuclear Schiff Moments and CP Violation

Jonathan Engel¹

¹Department of Physics and Astronomy, University of North Carolina, Chapel Hill, NC, 27516, USA, ; email: engelj@physics.unc.edu ; ORCID: 0000-0002-2748-6640

Keywords

CP violation, electric dipole moments, Schiff moments, nuclear-structure theory

Abstract

This paper reviews the calculation of nuclear Schiff moments, which one must know in order to interpret experiments that search for time-reversal-violating electric dipole moments in certain atoms and molecules. After briefly reviewing the connection between dipole moments and CP violation in and beyond the Standard Model of particle physics, Schiff's theorem, which concerns the screening of nuclear electric dipole moments by electrons, Schiff moments, and experiments to measure dipole moments in atoms and molecules, the paper examines attempts to compute Schiff moments in nuclei such as ^{199}Hg and octupole-deformed isotopes such as ^{225}Ra , which are particularly useful in experiments. It then turns to *ab initio* nuclear-structure theory, describing ways in which both the In-Medium Similarity Renormalization Group and coupled-cluster theory can be used to compute important Schiff moments more accurately than the less controlled methods that have been applied so far.

Contents

1. INTRODUCTION	2
2. EDMS AND CP VIOLATION	3
2.1. Beyond the CKM Matrix and Effective Couplings for Nuclear CP Violation	4
3. EDMS of ATOMS AND MOLECULES	5
3.1. Schiff's Theorem and Schiff Moments	6
3.2. Experiments in Atoms and Molecules	9
4. CALCULATIONS OF SCHIFF MOMENTS	10
4.1. Simple Estimate	10
4.2. Phenomenological Shell Model	11
4.3. Random Phase Approximation and Density-Functional Theory in Spherically Deformed Nuclei	12
4.4. Comparison of Results	14
4.5. A Special Case: Octupole Deformed Nuclei	15
5. THE NEAR FUTURE: AB INITIO CALCULATIONS	18
5.1. Ab Initio Many-Body Methods	18
5.2. In-Medium Similarity Renormalization Group	19
5.3. Coupled-Cluster Method	21
6. Conclusion	21

1. INTRODUCTION

It is a strange time for the field of fundamental physics. There is no shortage either of unexplained phenomena or of theoretical puzzles. We still do not know what dark matter is made of, we understand little about dark energy, and we cannot explain why the universe contains so many more baryons than anti-baryons, an imbalance that is difficult to chalk up to an initial condition if inflation takes place (1). Sakharov famously pointed out (2) that a phase transition in concert with a source of CP violation could explain the asymmetry, but by all accounts the one known source of CP violation, a phase in the Cabibbo-Kobayashi-Maskawa (CKM) matrix that mixes quark mass and flavor eigenstates (3), is too weak. For this reason, and because global symmetries such as CP are often not regarded as natural, many people suspect that nature violates CP invariance more strongly than does the CKM phase. This additional CP-violating physics has not, of course, been seen in high-energy experiments. As we shall see shortly, however, static electric dipole moments (EDMs) in atoms and molecules without a lot of degeneracy violate time-reversal (T) symmetry, which implies CP violation (4), and experiments to measure EDMs are both exquisitely sensitive and becoming even more sensitive at a rapid pace. Such experiments may thus provide our best chance to discover a new source of CP violation.

One mystery is that there is an additional potential source of CP violation in the standard model that isn't doing the job it might: the term in the QCD Lagrangian with the form

$$\mathcal{L}_{\bar{\theta}} = -\frac{g^2}{16\pi^2} \bar{\theta} \text{Tr} \left(G^{\mu\nu} \tilde{G}_{\mu\nu} \right), \quad 1.$$

where $\bar{\theta}$ includes the effects of CP-violating angles in the quark mass matrix that we assume have been rotated away. The QCD CP violation should cause the neutron (as well as atoms and molecules) to have an EDM, but experiments (5) show that its EDM is less than about

$1.8 \times 10^{-26} e \text{ cm}$. That result implies that $\bar{\theta} \lesssim 10^{-10}$, a value so small that it seems to require an explanation. Although many have been offered (6, 7) — the presence of new particles called axions is probably the most popular (8, 9, 10) — none have been shown to be correct.

Whatever the ultimate source of non-CKM CP violation might be, its presence would cause atomic or molecular EDMs, the concern in this paper, that reflect T-violating properties either of the electron or of the atomic nucleus (or of both). In the second case, the nucleus would induce an EDM in the system that contains it through its interaction with the electrons. As we shall see, the nuclear physics responsible for this T-violating interaction can often be summarized in what is called the nuclear ‘‘Schiff moment,’’ which is a kind of radially weighted nuclear EDM. Our ability to interpret an observation (or non-observation) of an atomic or molecular EDM depends on understanding the dependence of the nuclear Schiff moment on the underlying source of CP violation. Though particle theory, QCD, and effective field theory are all required to make the connection, nuclear-structure theory is particularly important because the uncertainty associated with its methods is particularly large and because the field is poised to reduce that uncertainty significantly. The delicate nuclear structure that affects Schiff moments will therefore be the central topic of this review.

2. EDMS AND CP VIOLATION

Why do electric dipole moments violate T? The argument is a little different from the usual quantum-mechanical one that depends only on the commutation of the Hamiltonian with a symmetry operator. The electric-dipole operator in quantum mechanics,

$$\mathbf{D} = \sum_i q_i \mathbf{r}_i, \quad 2.$$

where the index i labels particles, q_i is the charge of the i^{th} particle, and \mathbf{r}_i is its position vector, has negative parity. As a result, by the usual kind of argument, parity conservation implies that a static dipole moment in a state without any degeneracy beyond that caused by rotational symmetry must vanish. Though the demonstration is a little more involved, the conservation of time-reversal symmetry implies the same thing, with or without parity conservation (11).

The argument goes as follows: The time-reversal operator T , because it reverses angular momenta, takes normalized states with well defined angular momentum J and projection M into normalized states with J and $-M$. Thus, if time-reversal symmetry is conserved, one must have within a rotational multiplet $|J, M\rangle$ of definite energy,

$$\begin{aligned} \langle J, M | D_z | J, M \rangle &= \langle J, M | T^{-1} T D_z T^{-1} T | J, M \rangle \\ &= \langle J, -M | T D_z T^{-1} | J, -M \rangle \\ &= \langle J, -M | D_z | J, -M \rangle, \end{aligned} \quad 3.$$

where the last equality holds because \mathbf{D} , which depends only on positions, is even under time reversal. The operator R_π that rotates around the x axis by π also takes $|J, M\rangle$ to a phase times $|J, -M\rangle$, but \mathbf{D} is odd under this operation. Thus

$$\begin{aligned} \langle J, M | D_z | J, M \rangle &= \langle J, M | R_\pi^{-1} R_\pi D_z R_\pi^{-1} R_\pi | J, M \rangle \\ &= -\langle J, -M | D_z | J, -M \rangle. \end{aligned} \quad 4.$$

Equations 3 and 4 together imply that $\langle J, M | D_z | J, M \rangle = 0$. The argument breaks down if time-reversal symmetry is violated because in that case the state $|J, -M\rangle$ in the second and third lines of Eq. 3 need not belong entirely to the same rotational multiplet as the state $|J, M\rangle$, and thus need not be the same state as $|J, -M\rangle$ in Eq. 4.

Because of the CPT theorem, a nonzero EDM for a state with no degeneracy beyond that in M implies that CP symmetry is violated. Not only that, for years to come, a detectable EDM will have to be caused by $\mathcal{L}_{\bar{\theta}}$ or physics beyond the Standard Model, even with the amazing experimental sensitivity that is already possible. The reason is that the CKM phase causes a change of flavor and so flavor-diagonal quantities such as EDMs require Feynman diagrams with several loops to produce a non-zero result. **Figure 1** below shows one of the leading diagrams (12) in the expression for the neutron EDM, which the result of a full calculation reveals (13) to be about $10^{-32}e$ cm. Experiments looking for a new flavor-conserving source of CP violation will have to increase their sensitivity by several orders of magnitude before background from the CKM phase becomes an issue.

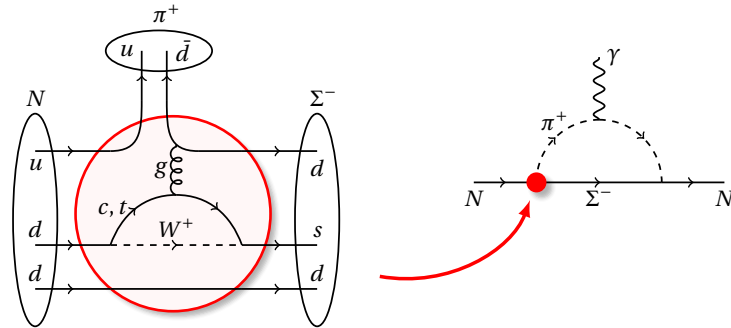


Figure 1

A leading diagram in the Standard Model for the neutron EDM caused by the CKM phase. Lower-case letters on the left label quark flavors, W labels a charged weak boson, and the ellipses represent the collection of valence quarks that make up the neutron (N), pion (π), and strange baryon (Σ). The red circle on the right contains the corresponding larger circle on the left. The wavy line labeled γ represents a photon.

Physics from beyond the Standard Model could produce much larger EDMs. Theories of new physics typically generate EDMs at one or two loops, and experiments on the neutron are already sensitive to new physics at the TeV scale for one-loop diagrams. Experiments on the electron EDM (14) are sensitive (15) at present to a new-physics scale of perhaps 50 TeV (for one loop diagrams) or 2 TeV (for two loop diagrams), and, as just noted, have orders of magnitude room to improve before background from CKM CP violation makes discovering new physics harder.

2.1. Beyond the CKM Matrix and Effective Couplings for Nuclear CP Violation

We see that EDMs are sensitive to new sources of CP violation, but how do we compute the EDMs predicted by possible new sources? If we had to do the full calculation for each theory of new physics we'd be in trouble, but we can use a hierarchy of energy scales — fundamental physics at and above the TeV scale, the Standard Model at a hundred GeV or so, mesons and nucleons at about 1 GeV, nuclei at the MeV scale, and atoms at the eV

scale — to divide the work so that the missing information at each level can be summarized in a few unknown parameters.

Here we will be interested in atomic and molecular EDMs that are induced by physics inside atomic nuclei. At the nuclear level, the framework that makes a parameterization of higher-scale physics possible is chiral effective field theory (χ EFT), which expands the most general pion and nucleon Lagrangian that is consistent with spontaneously-broken chiral symmetry in powers of p/Λ and m_π/Λ , where p is a typical momentum for a nucleon in a nucleus, m_π is the pion mass, and Λ is the scale at which the dynamics of degrees of freedom beyond pions and nucleons become important (16, 17, 18).

At leading order in χ EFT, the usual strong nuclear potential contains one-pion-exchange and contact nucleon-nucleon interactions. The same is often true of the leading-order P- and T-violating potential V_{PT} (19, 20), though exactly which terms are leading depends on the underlying sources of CP violation. With the use of the strong pion-nucleon coupling $g \approx 13.3$ in the definition instead of $g_A m_N / f_\pi$, which is equal to g to within a few percent, the pion-exchange part (always occurring at leading order) is

$$V_{PT}^\pi(\mathbf{r}_1 - \mathbf{r}_2) = \frac{g}{2m_N} \left\{ [\bar{g}_0 \vec{\tau}_1 \cdot \vec{\tau}_2 + \bar{g}_2 (3\tau_{1z}\tau_{2z} - \vec{\tau}_1 \cdot \vec{\tau}_2)] (\boldsymbol{\sigma}_1 - \boldsymbol{\sigma}_2) - \bar{g}_1 (\boldsymbol{\sigma}_1 \tau_{1z} - \boldsymbol{\sigma}_2 \tau_{2z}) \right\} \cdot \nabla Y(|\mathbf{r}_1 - \mathbf{r}_2|), \quad 5.$$

where

$$Y(r) = \frac{e^{-m_\pi r}}{4\pi r}, \quad 6.$$

and the \bar{g}_i are unknown CP-violating versions of g that depend on the underlying source of the violation. For special sources, e.g., the $\bar{\theta}$ term in Eq. 1, theorists have used lattice QCD to compute the constant \bar{g}_0 (21, 22), obtaining the value $\bar{g}_0 = (15.5 \pm 2.6) \times 10^{-3} \bar{\theta}$. The other couplings are harder to calculate, though Ref. (23) used resonance saturation to conclude, again for the $\bar{\theta}$ source, that $\bar{g}_1/\bar{g}_0 \approx -0.2$.

Pions are the pseudo-Goldstone bosons associated with the spontaneous breaking of chiral symmetry, and for sources of CP violation that conserve chiral symmetry at the quark and gluon level — i.e. in Standard-Model effective field theory — pion-exchange potentials of the form in Eq. 5 are suppressed. For such sources, a contact interaction with two parameters contributes at the same order as the suppressed pion exchange:

$$V_{PT}^\delta = \frac{1}{2} [\bar{C}_1 + \bar{C}_2 \boldsymbol{\tau}_1 \cdot \boldsymbol{\tau}_2] (\boldsymbol{\sigma}_1 - \boldsymbol{\sigma}_2) \cdot \nabla \delta^3(\mathbf{r}_1 - \mathbf{r}_2). \quad 7.$$

There are other contact interactions, not shown here, that never contribute at the same order as pion exchange. In addition, according to Standard-Model EFT, \bar{g}_2 is suppressed compared to \bar{g}_0 and \bar{g}_1 , no matter what the underlying source of CP violation. For a review of EFT for P- and T-violating interactions and operators, see Ref. (20).

The most important result of all these considerations for the interpretation of experiments on atoms or molecules is that we can proceed to compute the effects of nuclear CP violation on EDMs as functions of a few important χ EFT parameters, without worrying about the underlying source of CP violation. We will see how to do so shortly.

3. EDMs of ATOMS AND MOLECULES

Atoms and molecules are easier to manipulate in a laboratory than lone hadrons or leptons. If CP is violated, the EDMs of those hadrons and leptons will contribute to an EDM for

the composite system. But the charge distribution of a composite system is also altered by the EDMs of its constituents, and one can ask whether the dipole moment of the new distribution will act to increase or reduce the summed EDMs of the constituents. The answer depends on whether the constituents are, like electrons, relativistic and spread out over the atomic/molecular volume or, like the nuclear constituents, confined to a much smaller volume. In the former case, the constituent EDMs can be enhanced, but in the latter they are dramatically screened. We will see how next.

3.1. Schiff's Theorem and Schiff Moments

Why are Schiff moments important? The reason is that nuclear EDMs are largely canceled by atomic electrons, which re-arrange themselves to create an EDM in the opposite direction. This result was first proved, not surprisingly, by Schiff in Ref. (24) and is presented in many other places (see, e.g., Refs. (25, 26) The proof here follows the discussion in Ref. (27), where more details are available. One begins by supposing that the nucleus has a dipole moment $\mathbf{d} = -e\mathbf{d}_0$, where e is the charge of the electron (the negative of the charge of the proton) and d_0 is a nuclear quantity — a ground-state expectation value — that has the dimension of length. With this assumption, one can write the atomic Hamiltonian in the form

$$H_{\text{atom}} = \sum_{i=1}^Z [T_i + V_i + e\phi(\mathbf{r}_i) - e\mathbf{E}_0 \cdot \mathbf{r}_i] + e\mathbf{E}_0 \cdot \mathbf{d}_0 \quad , \quad 8.$$

where T_i is the kinetic energy of the i^{th} electron ($p_i^2/2m_e$ in the nonrelativistic approximation, with m_e the electron mass), and \mathbf{r}_i and \mathbf{p}_i are that electrons' coordinates and momentum relative to the nuclear center of mass. In addition,

$$V_i = e^2 \sum_{j < i} \frac{1}{|\mathbf{r}_i - \mathbf{r}_j|} \quad 9.$$

is the electron-electron Coulomb interaction, and

$$\phi(\mathbf{r}_i) = -e \int \frac{d^3x \rho(\mathbf{x})}{|\mathbf{x} - \mathbf{r}_i|} \quad 10.$$

is the electrostatic potential due to the nuclear charge distribution $\rho(\mathbf{x})$, which is dimensionless and normalized to Z . One needn't worry about the internal nuclear Hamiltonian; $\rho(\mathbf{x})$ is just a nuclear-ground-state charge distribution. Virtual nuclear excitations turn out not to affect the conclusions reached here.

Now, transform the Hamiltonian by using the unitary operator

$$U = e^{iA}, \quad A = \frac{\mathbf{d}_0}{Z} \cdot \sum_{i=1}^Z \mathbf{p}_i. \quad 11.$$

Because d_0 is so small, the transformed Hamiltonian \bar{H}_{atom} , to the level of accuracy one needs, is $\bar{H}_{\text{atom}} \equiv UH U^{-1} \simeq H_{\text{atom}} + i[A, H_{\text{atom}}]$. The expectation value of the commutator $[A, H_{\text{atom}}]$ must vanish in any eigenstate of H_{atom} . Because the commutator of the momentum operator with of a function of \mathbf{r} is proportional to the gradient of that function, because the electric field is the negative of the gradient of the potential, and because the sum of the nuclear field vectors at the locations of all the electrons is the negative of

their combined field \mathbf{E}_e at the center of the nucleus, the ground-state expectation value of $[A, H_{\text{atom}}]$, in the limit that the nucleus is a point particle, gives

$$\langle \mathbf{d}_0 \cdot [\mathbf{E}_0 + \mathbf{E}_e] \rangle = 0. \quad 12.$$

Finally, because we could have used any vector in place of \mathbf{d}_0 in the operator A , this means that the external field causes the electrons to move so that the field they produce exactly cancels the external field at the nucleus. Thus, the point-nucleus's EDM does not affect the total energy to first order when the external field is turned on. The nuclear EDM is screened.

To see how the finite volume of the nucleus affects this screening, one can examine the transformed Hamiltonian \bar{H}_{atom} :

$$\begin{aligned} \bar{H}_{\text{atom}} &= \sum_{i=1}^Z (T_i + V_i - e\mathbf{E}_0 \cdot \mathbf{r}_i + e\bar{\varphi}(\mathbf{r}_i)) \\ \bar{\varphi}(\mathbf{r}) &= \phi(\mathbf{r}) + \frac{1}{Z} \mathbf{d}_0 \cdot \nabla \phi(\mathbf{r}). \end{aligned} \quad 13.$$

Although the internal nuclear Hamiltonian does not appear here, the nuclear radius R_N is still a relevant parameter because it characterizes $\rho(\mathbf{x})$, and it is much smaller than atomic radius R_A . Thus one can expand $\rho(\mathbf{x})$ in powers of $R_N/R_A \approx 10^{-4}$ and neglect all but the lowest few terms. The expansion is equivalent to an expansion in gradients of $\delta^3(\mathbf{x})$. In order to reproduce the lowest multipole moments, we write

$$\rho(\mathbf{x}) = \left[Z \delta^3(\mathbf{x}) + Z \frac{\langle r^2 \rangle_{\text{ch}}}{6} \nabla^2 \delta^3(\mathbf{x}) + \dots \right] - \left[\mathbf{d}_0 \cdot \nabla \delta^3(\mathbf{x}) + \frac{\mathbf{O}_0 \cdot \nabla}{10} \nabla^2 \delta^3(\mathbf{x}) + \dots \right] + \dots, \quad 14.$$

where $\langle r^2 \rangle_{\text{ch}}$ is the mean-square charge radius and

$$\mathbf{O}_0 = \int d^3x \mathbf{x} x^2 \rho(\mathbf{x}). \quad 15.$$

The vector quantity \mathbf{O}_0 , which is the second moment of the dipole distribution, bears a similar relationship to \mathbf{d}_0 as $Z \langle r^2 \rangle_{\text{ch}}$ does to Z . The terms in the second set of square brackets and higher terms with odd multipoles exist only if the nuclear Hamiltonian violates parity and time-reversal symmetry.

Now one can use the expression for the density in Eq. 14 to evaluate the modified potential $\bar{\varphi}$ in Eq. 13. One can write the potential as $\bar{\varphi} \equiv \varphi_0 + \bar{\varphi}_{PT}$, a sum of a term φ_0 that would be present even in the absence of nuclear P and T violation and another symmetry-violating term $\bar{\varphi}_{PT}$ that contains \mathbf{d}_0 or \mathbf{O}_0 , obtaining

$$\begin{aligned} \bar{\varphi}_{PT}(\mathbf{r}) &= e \int d^3x \frac{[\mathbf{d}_0 \cdot \nabla \delta^3(\mathbf{x}) + \frac{1}{10} \mathbf{O}_0 \cdot \nabla \nabla^2 \delta^3(\mathbf{x})]}{|\mathbf{x} - \mathbf{r}|} \\ &\quad - e \frac{\mathbf{d}_0 \cdot \nabla}{Z} \int d^3x \frac{[Z \delta^3(\mathbf{x}) + \frac{1}{6} Z \langle r^2 \rangle_{\text{ch}} \nabla^2 \delta^3(\mathbf{x})]}{|\mathbf{x} - \mathbf{r}|} + \dots \\ &= 4\pi \mathbf{S} \cdot \nabla \delta^3(\mathbf{r}) \end{aligned} \quad 16.$$

The vector Schiff moment \mathbf{S} is given by

$$\mathbf{S} \equiv \frac{|e|}{10} \left(\mathbf{O}_0 - \frac{5}{3} \langle r^2 \rangle_{\text{ch}} \mathbf{d}_0 \right). \quad 17.$$

Thus, the coupling of the symmetry-violating part of the nuclear charge distribution to the atomic electrons is through the Schiff moment. The result (17) is of order R_N^3 , because the terms of order R_N cancel in Eq. 16.

As we've seen, the density $\rho(x)$ comes ultimately from the nuclear ground-state wave function, and one can easily write an operator whose expectation value is the Schiff moment (using the exact same symbol, unfortunately). If one neglects properties of nucleons beyond their charges, the vector Schiff operator is

$$\mathbf{S}^{\text{ch}} = \frac{|e|}{10} \sum_{i=1}^Z \left(r_i^2 - \frac{5}{3} \langle r^2 \rangle_{\text{ch}} \right) \mathbf{r}_i, \quad 18.$$

where the sum is over protons. To treat the effects of dipole moments for the nucleons, one must add to the Schiff operator a ‘‘nucleon’’ piece

$$\mathbf{S}^n = \frac{1}{6} \sum_{i=1}^A (r_i^2 - \langle r^2 \rangle_{\text{ch}}) \mathbf{d}_i \quad 19.$$

where now the sum is over all nucleons and the \mathbf{d}_i are operators that, by the Wigner-Eckart theorem, must have the form $\mathbf{d}_i = D_i \boldsymbol{\sigma}_i$. The coefficients D_i must have one value for all protons i and another (possibly the same) for all neutrons i . Both the above equations omit a small piece with quadrupole character and a term of order $(Z\alpha)^2$ that is due to relativity in electron wave functions (28) as well, perhaps, as more subtle electron-nucleus interactions (29).

Because \mathbf{S}^{ch} and \mathbf{S}^n are vectors, a nonzero Schiff moment requires the nuclear ground state to actually be a multiplet $|\tilde{g}; J, M\rangle$ of $2J + 1$ states with different values for the z projection of the total angular momentum $J \geq 1/2$. (Here g stands for ‘‘ground state’’ and the tilde indicates the presence of V_{PT} in the Hamiltonian.) In such a case, one *defines* the Schiff moment to be the expectation value of the z component of the total Schiff operator $\mathbf{S} \equiv \mathbf{S}^{\text{ch}} + \mathbf{S}^n$ in the state with $M = J$, viz.,

$$S = \langle S_z \rangle_{\tilde{g}; J, J}, \quad 20.$$

where the subscripts after the semicolon indicate the values of the total angular momentum and its z projection. In perturbation theory in V_{PT} , which is essentially exact given the weakness of that interaction, the Schiff moment of the nuclear ground-state multiplet $|\tilde{g}; J, M\rangle$ that without the perturbation becomes $|g; J^\pi, M\rangle$ (the ‘‘g’’ has no tilde and the states have good parity π) can be written as

$$S = \sum_n \frac{\langle g | S_z | n \rangle_{J, J} \langle n | V_{PT} | g \rangle_{J, J}}{E_g - E_n} + c.c., \quad 21.$$

where the subscripts on the matrix elements contain the values of quantum numbers that are well defined in both the bra and ket. Because S is linear in V_{PT} , one can write, at leading order in χEFT ,

$$S = a_0 g \bar{g}_0 + a_1 g \bar{g}_1 + a_2 g \bar{g}_2 + A_1 \bar{C}_1 + A_2 \bar{C}_2 + a_p d_p + a_n d_n, \quad 22.$$

Here d_p and d_n are the nucleon dipole moments and the a 's and A 's contain all the nuclear physics. Given values for the V_{PT} couplings and the nucleon dipole moments, these

coefficients determine the Schiff moment, and it is the job of nuclear-structure theory to calculate them. Because of Schiff screening, experiments on free neutrons are more sensitive to a neutron EDM than are experiments in atoms and molecules. As a result, we will focus almost exclusively on S^{ch} , the part of the Schiff moment caused by V_{PT} , and in particular on T-violating pion exchange in V_{PT} , i.e., on a_0, a_1 , and a_2 .

One implication of our derivation of the Schiff theorem above is that an atomic EDM induced by the nucleus should be a factor of order $\left(\frac{R_N}{R_A}\right)^2 \approx 10^{-8} - 10^{-9}$ smaller than it would be without screening. In reality, though, the screening is not so strong. The large charge of heavy nuclei concentrates electrons at the nucleus, an effect that is enhanced by relativity, with the net result that the atomic EDM is reduced by the much smaller factor of about 10^{-3} . That's still a lot of suppression, but it can be overcome by experimental ingenuity.

It's worth noting that at higher order in the multipole expansion, other electric moments, such as the electric octupole, enter the expression for \vec{H}_{atom} . (The Schiff moment itself has a small correction involving the nuclear quadrupole moment.) Moreover, the nuclear current plays a role as well as the charge, and when the current's effect on electrons is worked out, one finds that the magnetic quadrupole moment is important (25, 30, 31, 32). Magnetic moments are unscreened and as a result, in nuclei with $J \geq 1$ and sufficient electron angular momentum, the atomic EDM induced by the nuclear magnetic quadrupole is usually larger, by an order of magnitude or more, than that induced by the Schiff moment. Magnetic quadrupole moments thus deserve a review of their own, or at least more space in a review like this one. Thus far, however, attempts to compute them have been much fewer, and so, while bearing in mind that in some experiments their effects will be the most important, they will not be considered further here.

3.2. Experiments in Atoms and Molecules

In heavy atoms, electron EDMs are not screened because they are in no way confined to a small sub-volume and the electronic motion is sufficiently relativistic. In paramagnetic atoms, which have unpaired electrons, electron EDMs can be greatly amplified. These atoms, however, offer no advantages for detecting nuclear CP violation unless it is in the form of a symmetry-violating nucleus-electron interaction, and will not be discussed.

Diamagnetic atoms do not accentuate electron EDMs and so are useful for detecting CP violation within the nucleus. Some of the best limits on atomic EDMs come from experiments in diamagnetic atoms. The most sensitive (33, 34), on the atom containing the isotope ^{199}Hg , has produced the result $|d| < 7.4 \times 10^{-30} e\text{cm}$. A strong limit also exists in ^{129}Xe : $|d| < 1.4 \times 10^{-27} e\text{cm}$ (35). Experiments on the octupole-deformed isotopes ^{225}Ra and ^{223}Ra have been underway for some time (36, 37) and, for reasons to be presented, have the potential to be more sensitive than experiments in isotopes with less exotic shapes.

In recent years, attention has moved to polar molecules, which generate internal electric fields that can be aligned with an external field to magnify its effects on EDMs. Such molecules can be either paramagnetic (14, 38, 39) or diamagnetic (40, 41), and thus be most sensitive either to electron EDMs or nuclear Schiff moments (or magnetic quadrupole moments). In the future, some of the latter will leverage the octupole deformation of one of the molecule's atoms (see Ref. (42) and references therein). The field's rapidly improving ability to cool and control atoms and molecules is exciting.

The problem for theory, of course, is extracting statements about the strength and likely

source of CP violation from the results of any of these experiments. For nuclear-structure theory, that means the computation of Schiff moments, the problem to which the rest of this paper is devoted.

4. CALCULATIONS OF SCHIFF MOMENTS

4.1. Simple Estimate

The simplest nuclear model in which to estimate the Schiff moment induced by the interaction V_{PT} is one in which the strong nucleon-nucleon interaction V can be represented by a mean-field U_0 and nucleons occupy simple spherical single-particle levels produced by the mean field. If one assumes that excitations of the nuclear core are not important in Eq. 21., then one can also replace the T-violating potential V_{PT} by a mean field. The simplest way to do that is to pretend that pions are heavy compared to an inverse nuclear radius (a gross approximation, but one that usually doesn't cause large errors in finite model spaces) so that $Y(r) \rightarrow 1/m_\pi^2 \delta^3(\mathbf{r})$; the spatial form of V_{PT}^π then becomes the same as that of V_{PT}^δ . Finally, with the assumptions that the neutron and proton densities are proportional, that the spin density is negligible compared to the number density, and that exchange terms in V_{PT}^π (as well as all terms in V_{PT}^δ) are unimportant, one arrives at the one-body parity- and time-reversal-violating potential (43, 44, 25):

$$U_{PT} = \frac{\varepsilon}{M_N m_\pi^2} \boldsymbol{\sigma} \cdot \nabla \rho \tau_z, \quad 23.$$

where ρ is the total nuclear density and

$$\varepsilon = \frac{g}{2} \left[\left(\frac{N-Z}{A} \right) (\bar{g}_0 + 2\bar{g}_2) - \bar{g}_1 \right]. \quad 24.$$

In spherical odd- A nuclei, in the crudest approximation, one can assume that all the nucleons but the last one of the odd system (neutrons or protons) form an inert ‘‘core’’ with total angular momentum zero. If one makes the final simplifications that the strong nuclear mean-field U_0 is dominated by a spin-independent part and that $\rho(r)$ and $U_0(r)$ are proportional, one can (as in some proofs of the Schiff theorem) exploit the fact that the perturbing Hamiltonian is proportional to $[\boldsymbol{\sigma} \cdot \mathbf{p}, U_0] = -i\boldsymbol{\sigma} \cdot \nabla U_0$ to analytically evaluate the sum in the perturbation-theory expression in Eq. 21 for the state of the last (valence) nucleon, obtaining

$$|\tilde{\psi}_{lj}\rangle = \left(1 + i\varepsilon \frac{\rho(0)}{M_N m_\pi^2 U_0(0)} \boldsymbol{\sigma} \cdot \mathbf{p} \right) |\psi_{lj}\rangle, \quad 25.$$

where $|\psi_{lj}\rangle$ is the valence eigenstate with orbital angular momentum l and total angular momentum j of the strong mean-field Hamiltonian. With this simple state, an estimate for $\rho(0)/U_0(0)$, and the further not totally unreasonable assumption that the $\langle \psi | r^2 | \psi \rangle \approx \frac{3}{5} R^2$, with $R = 1.1 \text{ fm} \times A^{1/3}$, Ref. (43) finds that the Schiff moment is zero for nuclei with an odd neutron and, translated into our notation, has a value of

$$S^{\text{ch}} \approx |e| \frac{[1 \pm (j + \frac{1}{2})]}{j + 1} A^{2/3} \times 10^{-2} \varepsilon \text{ fm}^3, \quad 26.$$

for nuclei with an odd proton, with the \pm corresponding to $l = j \pm 1/2$. One can extend this expression to deformed nuclei and relax some of the assumptions that enter it, but I will simply present it as a very rough generic estimate for Schiff moments (though the

moments in odd-neutron nuclei are not in reality systematically much smaller than those in odd-proton nuclei). One salient fact is the growth with A .

In nuclei that are not octupole deformed — such deformation is a special case that we’ll address later — it is possible to identify another simple physical phenomenon that affects Schiff moments: core polarization. The Schiff operator is a proton-only version of the isoscalar dipole operator, the experimental excitation spectrum of which has been studied occasionally (45, 46, 47). Much of the operator’s strength — the squared matrix element of the operator from the ground state to a given excited state — lies in a giant resonance above 20 MeV. Giant resonances suck strength away from low energies; in our context, a Schiff resonance above 20 MeV will reduce the ground-state Schiff moment (for a simple discussion, see Ref. (48).) Quantifying the degree of reduction requires more careful calculations, calculations which will be discussed later. For now, it is enough to note that the simple single-particle result for protons above is probably too large in most nuclei. The next section, turns to the natural generalization of the single-particle picture, the shell model.

4.2. Phenomenological Shell Model

The nuclear shell model (49, 50) has been applied to light, medium-mass, and heavy nuclei. It can work in deformed nuclei but in heavy deformed nuclei, the computational requirements can become extreme and the model is less often employed. For Schiff moments, only the not too deformed isotopes ^{129}Xe and ^{199}Hg have been treated in a version of the model (51, 52).

The shell model is a generalization of the single-particle picture that has a number of particles occupying a few valence harmonic-oscillator orbitals rather than just one particle occupying a single orbital. To obtain a system’s energy eigenstates, one must diagonalize a Hamiltonian in the space constructed from the valence orbitals. But because that space is only a small fraction of the full many-particle Hilbert space, the Hamiltonian that gives correct energies is different from the bare nuclear interaction. Methods for deriving this “effective interaction” exist (53, 54, 55, 56) but in the phenomenological version of the model, they are implemented only approximately or not at all, and at least parts of the effective interaction are fit to data in or near the nuclei under consideration. Ref. (51) works with interactions that begin with Brueckner G matrices (57) from phenomenological nucleon-nucleon potentials (58, 59, 60, 61) and adjust particular matrix elements to spectra. In principle, other operators, such as the Schiff operator, should also be replaced by effective versions. In the absence of measured Schiff moments, of course, that last step is difficult.

Even without such difficulties, using the shell model to accurately compute Schiff moments is a tall order. The unperturbed shell-model ground state $|g\rangle$ and low-lying excited states are determined by diagonalizing the effective Hamiltonian; the model often reproduces energies, electromagnetic moments, and transition rates exceptionally well. But to evaluate the perturbative sum in Eq. 21 one must include states n that lie well above and below the valence shell. The Schiff operator contains three powers of r , and as a consequence, its largest single-particle matrix elements are between states in the core or valence shell and others that lie three oscillator shells higher or lower. A coherent combination of these states make up the giant isoscalar/Schiff resonance discussed earlier. The energies and structures of such states can be obtained only very approximately in the shell model, which almost by definition focuses on the valence shell. Refs. (51, 52), following Ref. (62),

take those states to be the result of orthogonalizing individual particle-hole excitations of the ground state. In other words, the excitations are taken to be orthogonalized states with the schematic form $a_i^\dagger a_j |g\rangle$ and energy $\varepsilon_i - \varepsilon_j \gtrsim \hbar\omega$, where the ε 's are single-particle energies and $\hbar\omega$ is the energy difference between shells. The effects of such excitations are found to be small, but the error introduced by the simplified treatment is hard to quantify. Ref. (62) makes an attempt to examine the error in the energy denominators (and claims that it is small) but does not examine the error in the matrix elements that make up the numerators. The simple intermediate states that are assumed to be eigenvectors in this approach almost in reality mix, both with one another and with more complicated multi-particle multi-hole states that are completely absent. The random-phase approximation (RPA) and generalizations discussed in the next section explicitly capture at least some of this physics, which is the core polarization mentioned earlier. The results of shell-model Schiff-moment calculations appear after a discussion of these other methods, which is next.

4.3. Random Phase Approximation and Density-Functional Theory in Spherical or Symmetrically Deformed Nuclei

Nuclear density functional theory (DFT) is a variation of the Kohn-Sham approach used in atomic, molecular and condensed-matter theory. The energy-density functionals (EDFs) are obtained mainly by writing the contribution to the mean-field energy of a phenomenological nucleon-nucleon interaction as an integral involving the density matrix. If, like Skyrme interactions (63, 64), the potential has a range of zero, one ends up with a semi-local function of the density (local in the density and its derivatives except for the Coulomb piece, which comes from a long-range interaction). If the potential has a non-zero range, then only the direct (Hartree) part is local without further approximation. Once constructed, the functionals can be modified in ways that don't correspond to the mean-field expectation value of any underlying interaction. In spirit and much of practice, however, calculations with EDFs are variations on mean-field theory, either the Hartree-Fock (HF) approximation or its generalization, the Hartree-Fock-Bogoliubov (HFB) approximation that includes pairing correlations at the expense of breaking particle-number conservation.

The natural treatment of excited states within mean-field theory is the RPA or, within HFB, the quasiparticle random-phase approximation (QRPA). The usual “matrix” versions of the approaches involve the diagonalization of the residual Hamiltonian — the piece not incorporated into the average field — in a space consisting of a one-particle one-hole (or two-quasiparticle for the QRPA) and one-hole one-particle (two-quasihole) excitations of a not fully specified ground state. (It's hard to describe the method in a single sentence; please see, e.g., Refs. (65, 64)) The RPA energies and transition matrix elements turn out to be the same as one gets by computing the linear response of the Hartree-Fock ground state to a time-dependent perturbation, with the restriction that time-dependent state always remain a Slater determinant or quasiparticle vacuum. Excitation energies in this second picture correspond to poles in the response function and transition strengths to residues. For time-independent quantities such as the Schiff moment, in the case for which the energy functional is just the mean-field expectation value of a Skyrme Hamiltonian, the method for computing any of the coefficients a_i is simply to solve the mean field equations associated with the full Hamiltonian,

$$H = H_{\text{Skyrme}} + \lambda V_{PT}, \tag{27}$$

with the corresponding \bar{g}_i set to 1 and the others omitted. The dimensionless quantity λ

must be large enough to have a numerical effect but still small enough so that first-order perturbation theory is accurate. Once one has the solution, one evaluates $\langle S_z/\lambda \rangle$ directly as in Eq. 20. It is not hard to show (66) that the resulting Schiff moment is the same as that produced by the perturbative expression in Eq. 21 if the transition matrix elements in the latter are evaluated in the matrix (Q)RPA.

Very roughly speaking, there are two kinds of contributions to Eq. 21 in these schemes. In the first, V_{PT} affects only the last (valence) nucleon, like in the simple estimate above, yielding a non-zero result only in odd-proton nuclei. In the second, the last nucleon interacts with the others, which are paired and constitute a kind of core, leading to particle-hole excitations of the core. The unperturbed ground state gets much of its important structure in a similar way through the strong interaction of the last nucleon with the rest. These processes, or more precisely those that go beyond the excitation of uncorrelated one-particle one-hole states, are the core polarization already mentioned. The term perhaps makes most sense in the version of mean-field theory that includes V_{PT} through the direct evaluation of Eq. 20; I’ve noted that this approach is equivalent to the RPA. In it, the wave function of the core is polarized by the valence nucleon so that the mean field for the core changes its shape, spin properties, etc., and develops a Schiff moment itself.

The RPA is a flexible method that can be applied without the fully self-consistent mean field and Skyrme interactions that make up nuclear DFT. Refs. (67, 68) are good examples of that approach. To represent the mean field, the papers use Wood-Saxon potentials and their surface-peaked generalizations (for the spin-orbit potential) rather than starting with a two-body interaction and carrying out full HF or HFB calculations. For the *residual* two-body force, they use an unrelated zero-range Landau-Migdal interaction. The core polarization it causes always reduces the magnitude of the Schiff moment produced by the last proton alone in odd- Z nuclei (as in Eq. 26), or by the approximation to Eq. 21. (like that in the last section) in which the intermediate states are all uncorrelated proton one-particle-one-hole states in odd- N nuclei. (Both of these will be referred to as “independent-particle” moments.) Table 1 shows the reduction from independent-particle moments effected by the core polarization in the calculations of Ref. (67) in several isotopes either used in experiments or considered for use. These are all odd- N nuclei. Here and everywhere that follows, the independent-particle moments correspond to those in a mean-field approximation with genuine single-particle wave functions, not the estimate in Sec. 4.1, which involved several additional simplifications, in particular, the neglect even of uncorrelated proton particle-hole intermediate states.

As we’ve seen, core polarization is almost entirely absent from the large-scale shell-model calculations. A small amount is induced by the presence of more than one nucleon in the valence shell, but that is not enough to cause much quenching.

Table 1 Reduction of Schiff-moment coefficients a_i from the independent-particle approximation, in the calculations of Ref. (67).

	$a_0/a_0^{s.p.}$	$a_1/a_1^{s.p.}$	$a_2/a_2^{s.p.}$
^{199}Hg	0.004	0.61	0.05
^{129}Xe	0.13	0.10	0.08
^{211}Rn	0.16	-0.51	0.22
^{213}Rn	0.10	0.18	0.07

Table 2 The coefficients a_i , in units of $|e| \text{ fm}^3$, in ^{211}Rn from several nuclear-structure calculations.

Method	a_0	a_1	a_2
Independent particles (67)	0.12	0.12	0.24
Phenomenological RPA (67)	0.0019	-0.061	0.053
Skyrme linear response (66)	0.034 \leftrightarrow 0.042	-0.0004 \leftrightarrow -0.028	0.064 \leftrightarrow 0.078

Of course, there have also been fully self-consistent Skyrme QRPA calculations, both in the matrix version of the theory (69) and the linear-response version (66), in addition to the Wood-Saxon-based computations just presented. The scheme in Ref. (69) includes some correlations beyond those in the QRPA, and the calculation in Ref. (66), unlike all the others in mean-field theory, allows nuclear ground states to be deformed. Both sets of computations have been carried out with several different Skyrme functionals, from which there is no compelling reason to choose a favorite. The results of these calculations appear just below.

4.4. Comparison of Results

Table 2 shows the results from several papers for the coefficients a_i in Eq. 22, in the independent-particle approximation, the phenomenological RPA of Refs. (67) and (68), and the still phenomenological but fully self-consistent Skyrme linear-response (DFT) calculations for the spherical nucleus ^{211}Rn . The line for the last of these contains ranges because the calculations were done with several Skyrme functionals. Not very surprisingly, the last two methods agree fairly well and, also unsurprisingly, produce numbers that are quite quenched from the independent-particle results, with so much quenching in the isovector (a_1) channel that the sign of the coefficient changes.

Table 3 compares the results of more calculations for the crucial isotope ^{199}Hg . One can expect the numbers here to be less in accord because the isotope is unpleasantly complicated. Mean field calculations find it to be slightly deformed and very soft (72, 73), implying that a single mean field with oscillations around it, as in RPA-like treatments, may not be a very good approximation. And to the extent that a single mean field can be used, it may well correspond to a triaxial shape, to which the RPA-like methods have not been frequently applied. (The phenomenological RPA of Ref. (67) and the Skyrme matrix QRPA of Ref. (69) treat the nucleus as spherical, while the Skyrme linear-response approach of Ref. (66)

Table 3 The coefficients a_i , in units of $|e| \text{ fm}^3$, for ^{199}Hg from a variety of nuclear-structure calculations.

Method	a_0	a_1	a_2
Independent particles (44)	0.087	0.087	0.174
Pair-truncated shell model (70)	0.011	0.014	0.033
Pair-truncated shell model (71)	0.017	-0.016	0.066
Large-scale shell model (51)	0.080	0.078	0.15
Phenomenological RPA (68),(67)	0.00004	0.055	0.009
Skyrme QRPA (69)	0.002 \leftrightarrow 0.010	0.057 \leftrightarrow 0.090	0.011 \leftrightarrow 0.025
Skyrme linear response (66)	0.009 \leftrightarrow 0.041	-0.027 \leftrightarrow +0.005	0.009 \leftrightarrow 0.024

allows it to be deformed, but without breaking axial symmetry.) The shell model includes the dynamics of valence nucleons and is best suited for low-lying states in such nuclei but suffers, as we have seen, from a simplified treatment of the intermediate states in Eq. 21.

In the table, the large-scale shell model of Ref. (51) produces coefficients that are almost the same as the independent-particle estimates. The RPA-like calculations are the most quenched. For a_0 and a_2 , their predictions agree fairly well with one another and with those of the pair-truncated shell model (70), a computationally simpler version of the shell model that restricts the basis to states involving collective pairs. In the isovector channel, however, the linear-response method is in disagreement with the others, favoring numbers with the opposite sign. The method includes most of the same physics as the Skyrme QRPA, and the disagreement is not well understood. The spread of values is thus indeed large and one needs more reliable calculations. That the computation is delicate and difficult is not surprising. **Figure 2**, from Ref. (66) shows the computed parity-odd proton density induced by the \bar{g}_1 term in V_{PT} , in cylindrical coordinates. To obtain the Schiff moment, one must multiply this density change by $(r^2 - 5/3 \langle r^2 \rangle_{\text{ch}})z$ and integrate. It's hard to guess even what sign will result from such a calculation.

Reference (51) does suggest an explanation for the discrepancy between the results in different schemes. It notes that in addition to the $J^\pi = \frac{1}{2}^-$ ground state, ^{199}Hg has a low-lying excited state with the same quantum numbers. The calculated Schiff moment for the excited state is much smaller than that for the ground state. The paper's authors suggest that the mean field found, e.g., in Ref. (66) mistakenly contains a significant admixture of the low-lying excited state. That conjecture remains to be explored.

Table 4 shows results for ^{129}Xe , an isotope used in some experiments (35). As in ^{199}Hg , the shell model produces larger numbers than the other methods, though here even its numbers are quenched compared to those in the independent-particle picture. DFT has not been applied to this isotope.

4.5. A Special Case: Octupole Deformed Nuclei

There is one class of nuclei — those with pear-like shapes corresponding to octupole deformation — in which Schiff moments are greatly enhanced. Such nuclei are rare, but

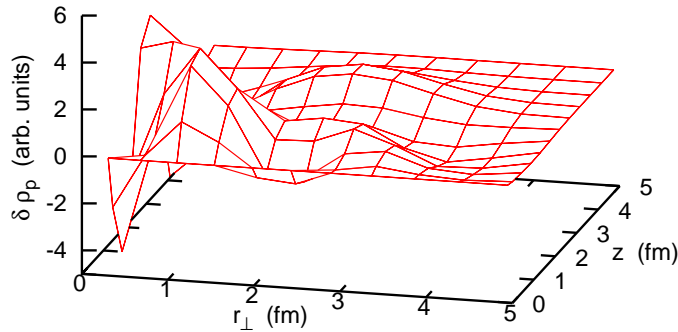


Figure 2

The change in proton density induced by the \bar{g}_1 term in V_{PT} , as a function of $r_\perp \equiv \sqrt{x^2 + y^2}$ and z . The units are arbitrary because of the arbitrariness in the constant \bar{g}_1 . Only a quarter of the density change is shown; it is symmetric in r_\perp and antisymmetric in z . (Taken from Ref. (66).)

Table 4 The same as Table 3, but for ^{129}Xe .

Method	a_0	a_1	a_2
Independent particles (44)	-0.11	-0.11	-0.22
Pair-truncated shell model (74)	0.0005	-0.004	0.0019
Pair-truncated shell model (62)	0.0032	-0.0012	0.0042
Large-scale shell model (51)	-0.038	-0.041	-0.081
Phenomenological RPA (67)	-0.008	-0.006	-0.009

regions of the isotopic chart, particularly the light-actinide region, contain them. **Figure 3** shows a Skyrme-HFB calculation (75) of the surface of the isotope ^{225}Ra . Nearby nuclei are similarly shaped.

To understand why the asymmetric shape leads to large Schiff moments, note that each rotational band in the spectrum of a rotating octupole has a partner band of opposite parity. In rigid odd- A nuclei, with body-fixed octupole-deformed mean fields, that statement means that every state has a degenerate partner with the same intrinsic structure but opposite parity; the two states are projections onto positive and negative parity of the same intrinsic body-frame state. Real nuclei are not perfectly rigid, of course, and in those that are octupole deformed one member of the doublet is lower in energy than its partner. The splitting can be quite small, however, compared to typical nuclear excitation energies.

The small splitting between partners in a parity doublet means that the partner of the ground state dominates the sum in Eq. 21. And the contribution of that state is even larger than the splitting suggests because the numerator contains $\langle g | S_z | \bar{g} \rangle_{J,J}$, where the bar denotes the parity-doublet partner. This quantity, up to a Clebsch-Gordan coefficient, is close to the intrinsic matrix element of \hat{S}_z , which is the classical Schiff moment of a charge distribution like that in Fig. 3. The moment is collective because the pear shape of the nuclear charge density comes from coherent contributions of many single-particle orbitals.

In the rigid-rotor limit, for which these statements are exact, and with the assumption that the contributions of all states but the parity-doublet partner are negligible, Eq. 21

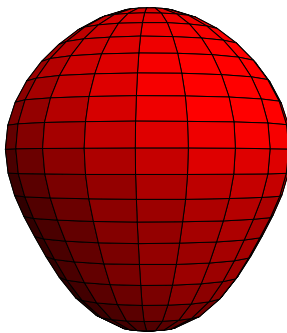


Figure 3

Shape of ^{225}Ra from the calculation of Ref. (76), represented by the surface of a uniform body with the same multipole moments as those of the calculated mass density (taken from Ref. (77)).

Table 5 The coefficients a_i , in units of $|e| \text{ fm}^3$ for ^{225}Ra from a several nuclear-structure calculations.

Method	a_0	a_1	a_2
Phen. octupole deformation (78)	2.7	-13.5	5.4
Skyrme DFT (75)	1.0 \leftrightarrow 4.7	-6.0 \leftrightarrow -21.5	3.9 \leftrightarrow 11.0
Constrained Skyrme DFT (77)	-0.4 \leftrightarrow 0.8	-2.0 \leftrightarrow -8.0	1.8 \leftrightarrow 4.8

becomes

$$\begin{aligned}
 S &\approx \frac{\langle g|S_z|\bar{g}\rangle_{J,J} \langle \bar{g}|V_{PT}|g\rangle_{J,J}}{E_g - E_{\bar{g}}} + c.c. \\
 &= -2 \frac{J}{J+1} \frac{\langle S_z \rangle_{\text{int}} \langle V_{PT} \rangle_{\text{int}}}{\Delta E},
 \end{aligned}
 \tag{28}$$

where $\Delta E = E_{\bar{g}} - E_g$ and the subscript ‘‘int’’ refers to the intrinsic symmetry-breaking state. All that must be computed, then, are the intrinsic ground-state matrix elements of S_z and V_{PT} . Despite the simplicity of this description, however, an equally simple estimate of the size of S is not so easy to obtain. Although ΔE can be taken from experiment and $\langle S_z \rangle_{\text{int}}$ related to other experiments in a way to be described shortly, $\langle V_{PT} \rangle$ is a more delicate quantity. Results of more than one kind of calculation nonetheless show that the Schiff moment of ^{225}Ra is much larger than that of ^{199}Hg .

Table 5 shows the results of these calculations for ^{225}Ra . The first is from a particle-rotor model in Ref. (78), the authors of which first pointed out the octupole enhancement (79, 80). They used an octupole-deformed Wood-Saxon potential from the semi-self-consistent work in Ref. (81), to calculate the intrinsic matrix elements in the last line of Eq. 28 and took $\Delta E = 55 \text{ keV}$ from experiment. The second set of results is from Skyrme HFB calculations of the same quantities, with ΔE again taken from experiment. The range in the table corresponds, as for ^{199}Hg , to the spread in the predictions of several Skyrme functionals.

The source of the last line, from Ref. (77), requires a slightly longer description. That paper shows that the intrinsic Schiff moment in Eq. 28 is very tightly correlated with the intrinsic octupole moment associated with the operator $\sum_{i=1}^Z r_i^3 Y_0^3(\theta_i, \varphi_i)$; the predictions for the two quantities by all Skyrme functionals lie on a straight line when plotted versus one another. The intrinsic expectation value of V_{PT} , the other quantity in Eq. 28 is not very correlated with the octupole moment, but the product of the two factors retains a correlation. **Figure 4** plots the coefficients a_i produced by HFB calculations with six Skyrme functionals, along with the experimental intrinsic octupole moment, obtained from measured E2 and E3 transition strengths (82). Although the correlation is not perfect, it exists, and by interpolating the results so that they reproduce the measured octupole moment, one obtains predictions for the coefficients. The last line in Tab. 5 comes from a similar analysis in which the measured octupole moments in both ^{224}Ra and ^{226}Ra (83) are used in the fit.

A comparison of Tab. 5 with Tab. 3 indeed reveals a large enhancement for ^{225}Ra . Other octupole-deformed light actinides also have enhanced Schiff moments, and polar molecules containing them have recently become attractive for experiment.

The first and second lines of Tab. 5 are different from what was reported in the review article, Ref. (84). The reasons are a mistaken expression for ε in Eq. 24 in that paper, and sign errors in Ref. (75).

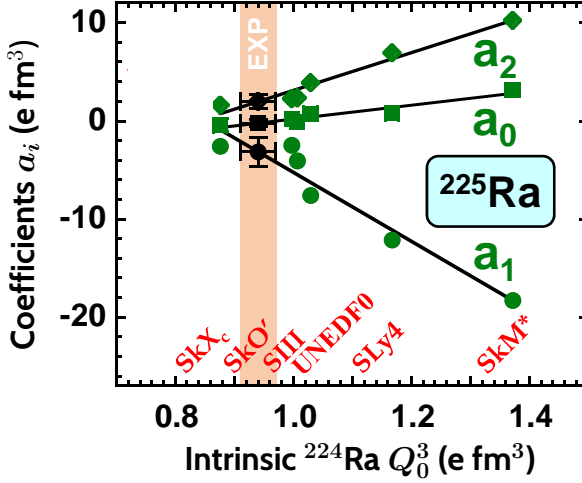


Figure 4

Coefficients a_i , in units of $|e| \text{ fm}^3$, in ^{225}Ra for six Skyrme functionals and propagated to the measured octupole moment in ^{224}Ra

5. THE NEAR FUTURE: AB INITIO CALCULATIONS

We have already seen that χEFT determines the form of V_{PT} . It will also allow us to identify corrections to the Schiff operators in Eqs. 18 and 19. Such corrections will be much smaller, however, than the inaccuracies in calculated Schiff moments coming from approximate solutions of the kind presented above to the nuclear many-body problem. Here we examine ways in which those solutions can become more accurate in the next few years. The program laid out parallels an effort, already underway, to improve the computation of nuclear matrix elements for neutrinoless double-beta decay (85).

5.1. Ab Initio Many-Body Methods

The development of χEFT and increases in the power of computers over the last 20 years have moved *ab initio* computation to the forefront of nuclear-structure theory. The term *ab initio* refers to calculations that start from Hamiltonians and other operators with forms specified by χEFT (usually), and coefficients most often fit to data from nucleon-nucleon scattering and properties of two- and three-nucleon systems such as the deuteron, triton, and ^3He . Once one has a strong and PT -violating Hamiltonian, the task of interest is to diagonalize the sum of the two of the two and compute the expectation value of S_z , either through Eq. 20 or Eq. 21.

Quantum Monte Carlo (86) is a scheme for evaluating the many-dimensional integrals that define a system's energy or time evolution. Several versions of the method have been applied to nuclear structure (87, 88). Green's function Monte Carlo (89) is the most accurate but is limited to nuclei lighter than about $A \approx 16$; the notorious sign problem leads to an exponential scaling of computing time with system size and limits the ability of many kinds of Monte Carlo to work in heavy nuclei. There, other more approximate methods with polynomial scaling have proved useful. These methods, while not exact, are "systematically improvable," meaning that they truncate correlations and can be made arbitrarily accurate,

if more costly, by relaxing the truncation. Two such methods promise better calculations of Schiff moments: the In-Medium Similarity Renormalization Group (IMSRG) (90, 91), and the coupled-cluster method (92, 93). Both are discussed below.

5.2. In-Medium Similarity Renormalization Group

The IMSRG is a scheme for finding a unitary transformation of the *ab initio* nuclear Hamiltonian that decouples a low lying state or space of states from the rest of the many-body Hilbert space. The idea is to obtain the transformation in small steps, in a way that is similar to gradient descent. One does so by solving a differential “flow” equation,

$$\frac{d}{ds}H(s) = [\eta(s), H(s)] , \quad 29.$$

where s is a time-like flow parameter. Here $H(0)$ is the Hamiltonian that we are given. A number of options are available for the “generator” $\eta(s)$; one simple choice comes from dividing the Hamiltonian into a piece H_d that does not couple the space of low-lying states one cares about to the rest (d stands for “diagonal”), and a second piece, H_{od} , that does and that one wants to drive to zero. It’s straightforward to show that the generator

$$\eta(s) = [H_d(s), H_{od}(s)] , \quad 30.$$

does the trick, with the effective Hamiltonian in the low-lying space given by the projection onto that space of $H_d(\infty)$. Other generators that do the same job are better in practice because the flow equations that they produce are not as stiff (90).

No matter what generator one chooses, however, Eq. 29 is too hard to solve exactly. $H(0)$ and $\eta(0)$ both contain two-body pieces and sometimes three-body pieces, and as a result $H(s)$ develops up to A -body pieces. One must truncate at the two-body or three-body level, after normal-ordering with respect to the “reference” state or ensemble of states that one wishes to decouple. (The normal ordering is crucial; it incorporates the parts of higher-body interactions that have a non-zero reference expectation value.). The simplest version of the method decouples a single reference Slater determinant. The valence space version (denoted by the acronym VS-IMSRG) decouples all the states constructed from valence nucleons in one or two shells (94). Finally, the “In-Medium Generator-Coordinate Method” (IM-GCM) approximately decouples a single correlated state or ensemble constructed through the use of generator coordinates such as deformation parameters and pairing gaps (95). The VS-IMSRG promises accurate Schiff moments in soft nearly spherical nuclei such as ^{199}Hg and the IM-GCM does the same in octupole-deformed nuclei such as ^{225}Ra . The two approaches will be considered in turn.

5.2.1. Valence-Space IMSRG and Near-Spherical Nuclei. We have seen that the shell model can describe the low-lying structure of ^{129}Xe and ^{199}Hg , but has trouble including the core polarization induced by high-energy intermediate states in Eq. 21. The IMSRG, however, can incorporate physics at high energies into valence-space Hamiltonians and moments. If, as in Eq. 27., one writes the full Hamiltonian in the form

$$H(s) = H_0(s) + \lambda V_{PT}(s) \quad 31.$$

where H_0 is the strong Hamiltonian, and write the generator as

$$\eta(s) = \eta_0(s) + \lambda \eta_{PT}(s) , \quad 32.$$

one can expand the flow equations to first order in λ to obtain

$$\frac{dH_0(s)}{ds} = [\eta_0(s), H_0(s)] \quad 33.$$

and

$$\frac{dV_{PT}(s)}{ds} = [\eta_{PT}(s), H_0(s)] + [\eta_0(s), V_{PT}(s)]. \quad 34.$$

The first of these equations is just the usual IMSRG flow; the second evolves V_{PT} to an effective version for use in the valence shell. After solving these, one can transform the Schiff operator in a similar way and use the effective valence Hamiltonian and Schiff operator to compute the Schiff moment. The effects of the intermediate states outside the model space should be captured by these effective operators.

When the commutators in the flow equation are truncated at the one-body level, after normal ordering, the IMSRG with a Slater determinant reference state is similar to the HF approximation (90); it decouples all one-particle one-hole states from the reference. Recall from Section 4.3 that the linear-response DFT computation of the static Schiff moment reduces to a mean-field calculation with V_{PT} included. The implication is that the IMSRG should include all the physics of that calculation, plus additional correlations from truncating at the two-or-three-body normal-ordered level instead of the one-body level and using a strong Hamiltonian from χ EFT. We anticipate useful *ab initio* Schiff moments in ^{199}Hg and ^{129}Xe from this scheme.

5.2.2. IM-GCM and Octupole-Deformed Nuclei. Pear-shaped nuclei are so exotically deformed that one or two valence shells are not sufficient even to treat them approximately. But, as we saw in Section 4.5, we need only the ground-state and its opposite parity partner to compute the Schiff moment. The IM-GCM, which focuses on just a few low-lying collective states, is thus the version of the IMSRG that is best suited for the computation.

The IM-GCM applies methods such as symmetry-breaking mean-field theory and the projection of symmetry-broken states onto their unbroken counterparts that were developed in nuclear DFT. (It also allows the mixing of different mean fields, which is the essence of the generator-coordinate method.) Thus, just as the ideas in DFT response calculations can be incorporated into the VS-IMSRG, the spontaneous parity-breaking DFT calculations described in Sec. 4.5 can be generalized in the IM-GCM. A good IM-GCM calculation will start with a parity- and rotational-symmetry-breaking HF or HFB calculation, with projection of the resulting quasiparticle vacuum onto states with the quantum numbers of the ground state and its partner creating a two-state ensemble that can serve as the reference for normal ordering. (Ensemble normal ordering is used both in the VS-IMSRG(94) and in the application of the IM-GCM to double-beta decay (95, 96).) After creating the reference, one can solve the corresponding flow equations and use the first line of Eq. 28 to compute the Schiff moment. Because normal ordering with respect to a complicated state or ensemble is different from ordering with respect to a Slater determinant, the flow equations do not fully decouple the reference and are followed by a re-diagonalization of the Hamiltonian, in a space consisting of the reference states plus the most important non-reference states; at the end, one will use Eq. 28. again.

There are no major obstacles in the path to a computation of the Schiff moment of ^{225}Ra .

5.3. Coupled-Cluster Method

The coupled-cluster method has a long history, beginning in nuclear physics (97), then undergoing extensive development in atomic and molecular physics/chemistry (98), and finally returning to nuclear physics (93, 99) some 20 years ago. Within nuclear physics, it has been applied even in nuclei as heavy as ^{208}Pb (100), and to processes ranging from photo-absorption (101) to double-beta decay (102).

The basic idea of the approach is to write the nuclear ground state in the completely general form,

$$|g\rangle = e^T |\Phi\rangle, \quad 35.$$

where $|\Phi\rangle$ is a Slater determinant and

$$T = \sum_{mi} t_i^m a_m^\dagger a_i + \sum_{mni} t_{ij}^{mn} a_m^\dagger a_n^\dagger a_i a_j + \dots, \quad 36.$$

where m, n, \dots label particle orbits and i, j, \dots hole orbits and the t 's are amplitudes. The expansion for T is truncated at the level indicated above or, sometimes, with three-body operators included as well. The exponentiation of T in Eq. 35, even when truncated, creates comprehensive correlations similar to those induced by the IMSRG flow equations.

Initially, nuclear coupled-cluster theory was used only in spherical isotopes, but recently, practitioners have developed a deformed-basis version of the method, with the operators in Eq. 36 creating and destroying deformed orbitals, and the ability to project rotational-symmetry-breaking states onto those with good angular momentum (103). Breaking and restoring parity symmetry will be a small step on top of that and will allow a computation of matrix elements of operators between members of a parity doublet. To mirror what is possible in the IM-GCM, it might also be necessary to break the U(1) symmetry that corresponds to particle-number conservation, as in HFB, in the theory's creation and annihilation operators. A quasiparticle coupled-clusters theory has been developed (104, 105), but not yet combined with the version that allows deformation. As with the IM-GCM, however, there appear to be no insurmountable obstacles to an accurate calculation of the Schiff moment of ^{225}Ra .

6. Conclusion

This article has been meant to show both the importance of computing nuclear Schiff moments and the difficulty in doing so well. A variety of traditional methods have been applied to the problem, with success that is hard to quantify. *Ab initio* methods promise more accurate results. Though the problem of estimating uncertainty hasn't been addressed here, Ref. (85) takes up the issue for calculations of neutrinoless double-beta decay, and a program similar to the one outlined there would be useful for Schiff moments as well. All the tools exist to advance the computation of these vital nuclear moments substantially in the next few years.

DISCLOSURE STATEMENT

The author is not aware of any affiliations, memberships, funding, or financial holdings that might be perceived as affecting the objectivity of this review.

ACKNOWLEDGMENTS

The author acknowledges the support of the US Department of Energy, Office of Nuclear Physics, under Grant No. DE-FG02-97ER41019, and coauthors S. Ban, P. Becker, M. Bender, J. Dobaczewski, J. Friar, A.C. Hayes, J.H. de Jesus, M. Kortelainen, C.P. Liu, M.J. Ramsey-Musolf, P. Olbratowski, and U. van Kolck, whose work contributed figures and results to this article. He also thanks collaborators A. Belley, D. Kekejian, B. Romeo Zaragozano, and R. Stroberg for enlightening conversations and useful work.

LITERATURE CITED

1. Coppi P. *eConf* C040802:L017 (2004)
2. Sakharov AD. *Soviet Physics Uspekhi* 34(5):392 (1991)
3. Kobayashi M, Maskawa T. *Prog. Theor. Phys.* 49:652–657 (1973)
4. Luders G. *Kong. Dan. Vid. Sel. Mat. Fys. Med.* 28N5(5):1–17 (1954)
5. Abel C, Afach S, Ayres NJ, Baker CA, Ban G, et al. *Phys. Rev. Lett.* 124(8):081803 (2020)
6. Nelson A. *Physics Letters B* 136(5):387–391 (1984)
7. Barr SM. *Phys. Rev. Lett.* 53(4):329–332 (1984)
8. Peccei RD, Quinn HR. *Phys. Rev. Lett.* 38(25):1440–1443 (1977)
9. Wilczek F. *Phys. Rev. Lett.* 40(5):279–282 (1978)
10. Weinberg S. *Phys. Rev. Lett.* 40(4):223–226 (1978)
11. Sachs RG. Chicago: Chicago Press (1987)
12. Shabalin E. *Sov. Phys. Usp.* 26:297 (1983)
13. Shindler A. *The European Physical Journal A* 57(4):128 (2021)
14. Andreev V, Ang DG, DeMille D, Doyle JM, Gabrielse G, et al. *Nature* 562(7727):355–360 (2018)
15. Alarcon R, et al. 2022. In *Snowmass 2021*
16. Leutwyler H. *Annals of Physics* 235(1):165–203 (1994)
17. Machleidt R, Entem DR. *Phys. Rept.* 503:1–75 (2011)
18. Epelbaum E, Krebs H, Reinert P. *Front. in Phys.* 8:98 (2020)
19. Maekawa C, Mereghetti E, de Vries J, van Kolck U. *Nucl. Phys. A* 872:117–160 (2011)
20. de Vries J, Epelbaum E, Girlanda L, Gnech A, Mereghetti E, Viviani M. *Frontiers in Physics* 8(July) (2020)
21. Borsanyi S, Durr S, Fodor Z, Hoelbling C, Katz SD, et al. *Science* 347(6229):1452–1455 (2015)
22. Brantley DA, Joo B, Mastropas EV, Mereghetti E, Monge-Camacho H, et al. Strong isospin violation and chiral logarithms in the baryon spectrum (2016)
23. Bsaisou J, Hanhart C, Liebig S, Meißner UG, Nogga A, Wirzba A. *The European Physical Journal A* 49(3):31 (2013)
24. Schiff L. *Phys. Rev.* 132:2194–2200 (1963)
25. Khriplovich I, Lamoreaux S. Berlin, Heidelberg: Springer-Verlag (1997), and references therein
26. Sen'kov RA, Auerbach N, Flambaum VV, Zelevinsky VG. *Phys. Rev. A* 77(1):014101 (2008)
27. Engel J, Friar J, Hayes A. *Phys. Rev. C* 61:035502 (2000)
28. Flambaum VV, Ginges JSM. *Phys. Rev. A* 65:032113 (2002)
29. Liu CP, Ramsey-Musolf M, Haxton W, Timmermans R, Dieperink A. *Phys. Rev. C* 76:035503 (2007)
30. Flambaum V. *Physics Letters B* 320(3):211–215 (1994)
31. Flambaum VV, DeMille D, Kozlov MG. *Phys. Rev. Lett.* 113(10):103003 (2014)
32. Lackenby BGC, Flambaum VV. *Phys. Rev. D* 98(11):115019 (2018)
33. Graner B, Chen Y, Lindahl EG, Heckel BR. *Phys. Rev. Lett.* 116(16):161601 (2016)
34. Graner B, Chen Y, Lindahl EG, Heckel BR. *Phys. Rev. Lett.* 119(11):119901 (2017)
35. Sachdeva N, Fan I, Babcock E, Burghoff M, Chupp TE, et al. *Phys. Rev. Lett.* 123(14):143003

- (2019)
36. Parker RH, Dietrich MR, Kalita MR, Lemke ND, Bailey KG, et al. *Phys. Rev. Lett.* 114(23):233002 (2015)
 37. Bishof M, Parker RH, Bailey KG, Greene JP, Holt RJ, et al. *Phys. Rev. C* 94(2):025501 (2016)
 38. Cairncross WB, Gresh DN, Grau M, Cossel KC, Roussy TS, et al. *Phys. Rev. Lett.* 119(15):153001 (2017)
 39. Hudson J, Kara D, Smallman I, Sauer B, Tarbutt M, et al. *Nature* 473:493–496 (2011)
 40. Grasdijk O, Timgren O, Kastelic J, Wright T, Lamoreaux S, et al. *Quantum Science and Technology* 6(4):044007 (2021)
 41. Denis M, Hao Y, Eliav E, Hutzler NR, Nayak MK, et al. *The Journal of Chemical Physics* 152(8):084303 (2020)
 42. Arrowsmith-Kron G, Athanasakis-Kaklamanakis M, Au M, Ballof J, Berger R, et al. *Reports on Progress in Physics* 87(8):084301 (2024)
 43. Flambaum V, Khriplovich I, Sushkov O. *Sov. Phys. JETP* 60:873 (1984)
 44. Flambaum V, Khriplovich I, Sushkov O. *Nucl. Phys. A* 449:750 (1986)
 45. Garg U. *Nuclear Physics A* 649(1):66–72 (1999), giant Resonances
 46. Uchida M, Sakaguchi H, Itoh M, Yosoi M, Kawabata T, et al. *Physics Letters B* 557:12 – 19 (2003)
 47. Clark HL, Lui YW, Youngblood DH. *Phys. Rev. C* 63:031301(R) (2001)
 48. Flambaum VV, Khriplovich IB, Sushkov OP. *Nucl. Phys. A* 449:750 (1986)
 49. Lawson R. Oxford Studies in Nuclear Physics Series. Clarendon Press (1980)
 50. Caurier E, Martínez-Pinedo G, Nowacki F, Poves A, Zuker AP. *Rev. Mod. Phys.* 77:427 (2005)
 51. Yanase K, Shimizu N. *Phys. Rev. C* 102(6):065502 (2020)
 52. Yanase K, Shimizu N, Higashiyama K, Yoshinaga N. *Physics Letters B* 841:137897 (2023)
 53. Kuo TTS, Osnes E. Springer-Verlag (1991)
 54. Hjorth-Jensen M, Kuo T, Osnes E. *Phys. Rep.* 261:125 (1995)
 55. Tsukiyama K, Bogner SK, Schwenk A. *Phys. Rev. C* 85:061304(R) (2012)
 - 56.
 57. Goldstone J. *Proceedings of the Royal Society of London. Series A, Mathematical and Physical Sciences* 239(1217):267–279 (1957)
 58. Kaya L, Vogt A, Reiter P, Siciliano M, Shimizu N, et al. *Phys. Rev. C* 100(2):024323 (2019)
 59. Utsuno, Yusuke, Otsuka, Takaharu, Shimizu, Noritaka, Honma, Michio, Mizusaki, Takahiro, et al. *EPJ Web of Conferences* 66:02106 (2014)
 60. Herling G, Kuo T. *Nuclear Physics A* 181(1):113–131 (1972)
 61. Blomqvist J, Rydström L, Liotta R, Pomar C. *Nuclear Physics A* 423(2):253–276 (1984)
 62. Teruya E, Yoshinaga N, Higashiyama K, Asahi K. *Phys. Rev. C* 96(1):015501 (2017)
 63. Skyrme T. *Nuclear Physics* 9:615 – 634 (1958-1959)
 64. Schunck N, ed. 2053-2563. IOP Publishing (2019)
 65. Ring P, Schuck P. Texts and Monographs in Physics. Springer (2004)
 66. Ban S, Engel J, Dobaczewski J, Shukla A. *Phys. Rev. C* 82:015501 (2010)
 67. Dmitriev VF, Sen'kov RA, Auerbach N. *Phys. Rev. C* 71:035501 (2005)
 68. Dmitriev VF, Sen'kov RA. *Phys. Atom. Nucl.* 66:1940 (2003)
 69. de Jesus J, Engel J. *Phys. Rev. C* 72:045503 (2005)
 70. Yoshinaga N, Teruya E, Higashiyama K, Yanase K. *JPS Conf. Proc.* 23:012034 (2018)
 71. Yoshinaga N, Yanase K, Higashiyama K. *Journal of Physics: Conference Series* 1643(1):012006 (2020)
 72. Prassa, Vaia, Karakatsanis, Konstantinos E., Lalazissis, George A. *EPJ Web Conf.* 252:02007 (2021)
 73. Patra SK, Yoshida S, Takigawa N, Prahara CR. *Phys. Rev. C* 50(4):1924–1931 (1994)
 74. Yoshinaga N, Higashiyama K, Arai R, Teruya E. *Phys. Rev. C* 87(4):044332 (2013)
 75. Dobaczewski J, Engel J. *Phys. Rev. Lett.* 94(23):232502 (2005)

76. Engel J, Bender M, Dobaczewski J, de Jesus JH, Olbratowski P. *Phys. Rev. C* 68:025501 (2003)
77. Dobaczewski J, Engel J, Kortelainen M, Becker P. *Phys. Rev. Lett.* 121(23):232501 (2018)
78. Spevak V, Auerbach N, Flambaum V. *Phys. Rev. C* 56:1357 (1997)
79. Spevak V, Auerbach N. *Phys. Lett. B* 359:254 (1995)
80. Auerbach N, Flambaum VV, Spevak V. *Phys. Rev. Lett.* 76(23):4316–4319 (1996)
81. Ćwiok S, Nazarewicz W. *Nuclear Physics A* 529(1):95–114 (1991)
82. Gaffney LP, Butler PA, Scheck M, Hayes AB, Wenander F, et al. *Nature* 497:199–204 (2013)
83. Wollersheim H, Emling H, Grein H, Kulesa R, Simon R, et al. *Nuclear Physics A* 556(2):261–280 (1993)
84. Engel J, Ramsey-Musolf MJ, van Kolck U. *Prog. Part. Nucl. Phys.* 71:21–74 (2013)
85. Cirigliano V, Davoudi Z, Engel J, Furnstahl RJ, Hagen G, et al. *Journal of Physics G: Nuclear and Particle Physics* 49(12):120502 (2022)
86. Nightingale M, Umrigar C. NATO ASI series: Mathematical and physical sciences. Springer Netherlands (1998)
87. Carlson J, Gandolfi S, Pederiva F, Pieper SC, Schiavilla R, et al. *Rev. Mod. Phys.* 87(3):1067–1118 (2015)
88. Gandolfi S, Lonardoni D, Lovato A, Piarulli M. *Frontiers in Physics* 8:117 (2020)
89. Carlson J. *Phys. Rev. C* 36(5):2026–2033 (1987)
90. Hergert H, Bogner SK, Morris TD, Schwenk A, Tsukiyama K. *Phys. Rep.* 621:165–222 (2016)
91. Hergert H. *Physica Scripta* 92:023002 (2016)
92. Shavitt I, Bartlett RJ. Cambridge Molecular Science. Cambridge University Press (2009)
93. Dean D, Hjorth-Jensen M. *Phys. Rev. C* 69:054320 (2003)
94. Stroberg SR, Calci A, Hergert H, Holt JD, Bogner SK, et al. *Phys. Rev. Lett.* 118(3):032502 (2017)
95. Yao JM, Engel J, Wang LJ, Jiao CF, Hergert H. *Phys. Rev. C* 98(5):054311 (2018)
96. Yao JM, Bally B, Engel J, Wirth R, Rodríguez TR, Hergert H. *Phys. Rev. Lett.* 124(23):232501 (2020)
97. Kummel H, Luhrmann KH, Zabolitzky JG. *Phys. Rept.* 36:1–36 (1978)
98. Crawford TD, III HFS. *Reviews in Computational Chemistry* 14:33 (2007)
99. Hagen G, Papenbrock T, Hjorth-Jensen M, Dean DJ. *Rept. Prog. Phys.* 77(9):096302 (2014)
100. Hu B, Jiang W, Miyagi T, Sun Z, Ekström A, et al. *Nature Physics* 18(10):1196–1200 (2022)
101. Bacca S, Barnea N, Hagen G, Orlandini G, Papenbrock T. *Phys. Rev. Lett.* 111(12):122502 (2013)
102. Novario S, Gysbers P, Engel J, Hagen G, Jansen GR, et al. *Phys. Rev. Lett.* 126(18):182502 (2021)
103. Hagen G, Novario SJ, Sun ZH, Papenbrock T, Jansen GR, et al. *Phys. Rev. C* 105(6):064311 (2022)
104. Henderson TM, Scuseria GE, Dukelsky J, Signoracci A, Duguet T. *Phys. Rev. C* 89(5):054305 (2014)
105. Signoracci A, Duguet T, Hagen G, Jansen GR. *Phys. Rev. C* 91(6):064320 (2015)